




Effect of the hole transporting layers on the inverted perovskite solar cells

Hanadi Mehdi^{1,*} , Muriel Matheron², Asya Mhamdi¹, Stéphane Cros², and Abdelaziz Bouazizi¹

¹Équipe Dispositifs Électroniques Organiques Et Photovoltaïque Moléculaire, Laboratoire de La Matière Condensée Et Des Nanosciences, Faculté Des Sciences de Monastir, Université de Monastir, Avenue de l'environnement, 5019 Monastir, Tunisia

²Université Grenoble Alpes, CEA, LITEN, INES, 73375 Le Bourget-du-Lac, France

Received: 28 May 2021

Accepted: 18 July 2021

Published online:
24 July 2021

© The Author(s), under exclusive licence to Springer Science+Business Media, LLC, part of Springer Nature 2021

ABSTRACT

Organic–inorganic hybrid perovskite solar cells have become one of the most promising photovoltaic technologies with conversion efficiency exceeding 25%. Increasing the efficiency of the perovskite solar cells is one of the most important challenges in the photovoltaic domain. The development of good hole transport layers (HTLs) is crucial for high-performance perovskite-based photovoltaic systems. Furthermore, it is important to accurately optimize the energy level matching between perovskites and hole transport materials via better charge collection. This work explores the effect of the HTLs on the growth process, morphology and crystallinity of the perovskite active layer and their impacts on the photovoltaic performance. Devices with planar inverted architecture ITO/HTL/MAPbI_{3-x}Cl_x/PC₆₀BM/BCP/Ag were fabricated using a one-step deposition method. The effects of the use of various HTL materials and the effect of the thermal annealing treatment of this layer were investigated. Morphological and microstructural analyzes of the perovskite films were carried out by scanning electron microscopy, X-ray diffraction. The optical properties in particular the absorption and the recombination process were studied by UV–vis absorption spectroscopy and photoluminescence spectroscopy. The photoelectric properties were investigated by photocurrent–voltage characteristic curves.

1 Introduction

Organic–inorganic lead halide perovskite-based solar cells (PSCs) have gained considerable attention in the past year due to their pleasing properties, namely, high absorption coefficients, adjustable bandgap and

lengths carrier diffusion in addition to the ease of elaboration [1–3]. Their conversion efficiency (PCE) has reached a dramatic improvement from 3.9% to currently 25.2% [4, 5], through interface modification [6, 7], charge transport layer design [8, 9], and composition engineering [10, 11], over the last few year. The planar heterojunction PSCs which are

Address correspondence to E-mail: hanadi.mehdi92@gmail.com

manufactured by stacking different planar thin films together have been implemented in two types of configurations, namely standard (n-i-p) and inverted (p-i-n) structures.

In fact, the p-i-n PSCs have attracted a lot of attention owing to their easy fabrication, to their metal oxide-free layers and to their cheap hole transporting materials [12, 13]. In addition, the inverted configuration use low processing temperature compared to standard configurations which mostly use the mesoporous TiO_2 as the ETL layer that requires a very high temperature. Moreover, the p-i-n PSCs can suppress the large hysteresis observed in standard structures [14].

The most research studies on the planar PSCs have focused on the optimizing the morphology of the perovskite active layer by controlling the crystallization process, such as the perovskite composition [15, 16], the methods of elaboration [17, 18], the annealing treatment [19, 20] and the additive engineering [21, 22]. To further improve the efficiency of the planar PSCs, efficient carriers transport to the hole transport layer (HTL) and the electron acceptor layer (ETL) is a critical requirement to demonstrate highly efficient planar solar cells. In general, fullerenes have been shown to be the most suitable candidate as an ETL layer in the inverted perovskite solar cells due to the fast and efficient charge transfer (0.40 ns) at the fullerene/perovskite interface [23, 24].

Considering the importance of the ETL layers, the HTLs play also an important role in the achievement of high efficiency and stable inverted PSCs by adjusting anodic working function, hole extraction and interfacial charge recombination [25, 26]. Much of research works have been interested in the study of the HTL materials, including the nature of the HTL materials, the doping of this layer [27–30]. Unfortunately, few of work that has been focused in the study of the annealing treatment of the HTL layer on the device's performance.

In this review, we report the elaboration of inverted perovskite solar cells based on $\text{MAPbI}_{3-x}\text{Cl}_x$ by a simple one-step spin coating process. The PSCs with the structure of ITO/HTLs/ $\text{MAPbI}_{3-x}\text{Cl}_x$ /PC₆₀BM/BCP/Ag were fabricated, in which the effects of the hole transport layer (HTL) were studied. The effect of the annealing time of the PEDOT: PSS layer was also investigated. Optical, morphological and structural properties were characterized and their effects on the performance were studied.

2 Experimental section

2.1 Materials

All the chemicals were used as received a without further purification, including lead chloride PbCl_2 (Sigma Aldrich), methylammonium iodide MAI (Lumttec), poly(3,4-ethylenedioxythiophene) polystyrene sulfonate PEDOT:PSS (PH1000) (Sigma Aldrich), poly[bis(4-phenyl)(2,4,6-trimethylphenyl)amine], Poly(triaryl amine) PTAA (Sigma Aldrich) and N-Dimethylformamide DMF (Sigma Aldrich).

2.2 Solar cell fabrication

First, the patterned ITO/glass substrate was cleaned by the sonication in acetone, isopropanol and deionized water successively. Then, the ITO substrate was dried by compressed N_2 flow and then putted through a UV-ozone treatment of 30 min before use. For the HTLs layer comparison, the PTAA (45 mm) was spin-coated at 2000 rpm for 40 (annealed at 100 °C for 20 min) and the PEDOT:PSS (40 mm) was spin-coated at 3000 rpm for 23 s (PEDOT: PSS at 180 °C for 60 min). After that, the $\text{CH}_3\text{NH}_3\text{PbI}_{3-x}\text{Cl}_x$ active layer was deposited on each HTL by one-step coating at 4000 rpm for 40 s, from solution containing 3:1 M ratio of methylammonium iodide (MAI) and lead chloride (II) (PbCl_2). The perovskite layers (thickness 225 nm) were followed by annealing treatment at 100 °C for 30 min. Then, the PC₆₀BM electron acceptor layers (15 mg/ml in chlorobenzene) were grown on the $\text{CH}_3\text{NH}_3\text{PbI}_{3-x}\text{Cl}_x$ active layers by one step spin coating at 1500 rpm for 60 s. Finally, the metal cathode of BCP (7 nm)/Ag (100 nm) was thermally evaporated in vacuum with a pressure of $< 10^{-5}$ Torr.

The schematic and energy band diagrams of the elaborated hybrid perovskite solar cells are shown in Fig. 1.

2.3 Device characterization

Optical characteristics were carried out using UV–vis absorption spectrophotometer Hitachi UV-2600 in the wavelength range from 400 to 800 nm with an integrating sphere. The steady-state photoluminescence spectra were obtained with a 4500-fluorescence spectrometer (selected wavelength $\lambda_{\text{exc}} = 500$ nm). The X-ray diffraction patterns of the thin films were

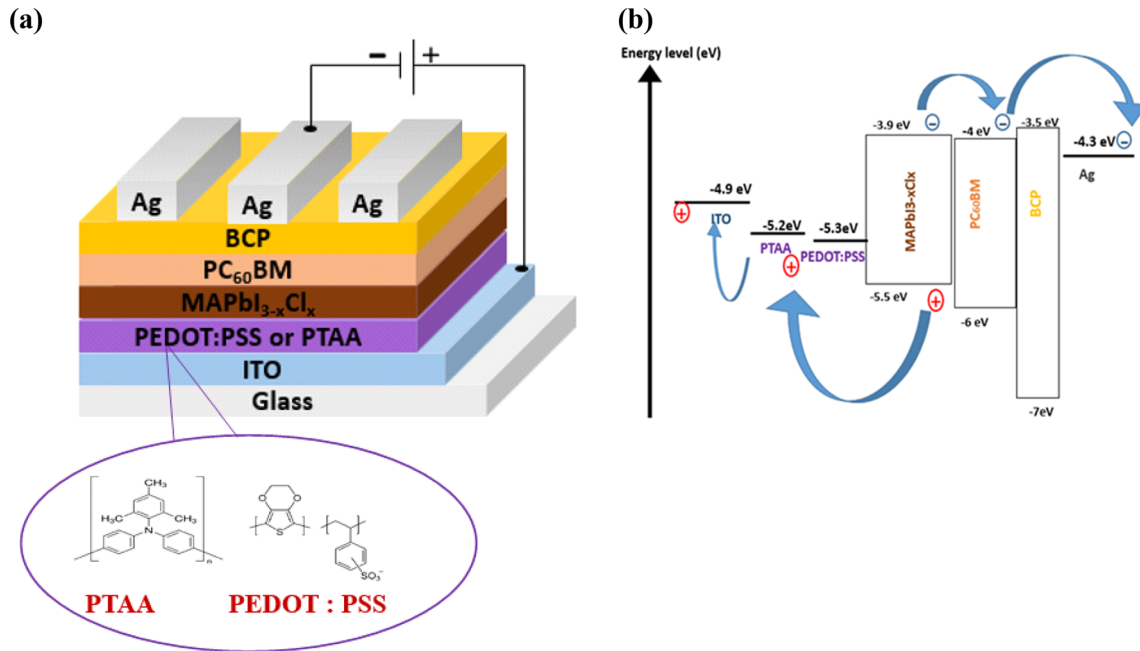


Fig. 1 **a** Device structure of ITO/HTLs/ MAPbI_{3-x}Cl_x/PC60BM/BCP/Ag solar cell. **b** schematic energy-level diagram

obtained using a Aeris PANalytical X-ray diffractometer equipped with Co K α ($\lambda = 1.79 \text{ \AA}$) radiation. For phase identification, diffraction peaks are converted to Cu using the following formula: $\sin\theta_{Cu} = (1.54/1.79) \sin\theta_{Co}$. The surface morphologies were inspected by scanning electron microscopy (SEM, LEO 1530). The photocurrent density–voltage (J–V) curves were obtained using a Keithley 2400 under the AM 1.5 G condition of 100 mW/cm^2 illumination.

3 Results and discussion

3.1 Nature of HTL material

The hole transporting material is an important active material in the inverted perovskite solar cells. It is the responsible of the hole’s extraction efficiency at the HTL / perovskite interface which can improve the performance of the device. Moreover, it can affect the crystal quality of the perovskite layer deposited above. In this part, we have studied the influence of the HTL material on the properties of the obtained perovskite films by studying two HTL materials PTAA and PEDOT: PSS.

3.1.1 Crystal phase

To study the crystal structure of the perovskite films deposited on different HTLs layers (PEDOT:PSS and PTAA), XRD analysis were carried out. As shown in Fig. 2, two strong peak at 16.14° and 33.05° assigned to (110) and (220) crystal planes of tetragonal MAPbI₃ perovskite phase were observed in all the perovskite films [20, 31], indicating the high crystalline quality of all the perovskite films. Additional prominent peaks at 17.88° and 36.53° corresponding to (100) and (310) planes were also shown. In addition, we note the

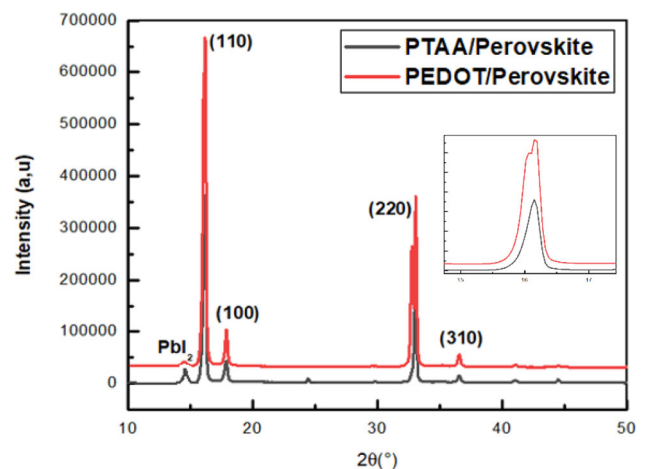


Fig. 2 X-ray diffraction patterns of PTAA/MAPbI_{3-x}Cl_x and PEDOT: PSS/MAPbI_{3-x}Cl_x on ITO substrates

presence of diffraction peak at 15.4° which was attributed to the PbI_2 lattice plane. Generally, this residual is located above the perovskite layer at the HTL / Perovskite layer interface. The presence of a large phase of PbI_2 appears to be detrimental because it can cause the charge carriers recombination at this interface, which subsequently affect the efficiency of the cells.

In situ the XRD measurements showed that the (110) and (220) peaks planes were significantly enhanced with the perovskite film deposited on PEDOT: PSS, suggesting the best crystallization process of the perovskite film.

The crystalline quality of the films can also be studied by calculating the size of the crystallites of the films using the Debye–Scherrer equation [32, 33] (Eq. 1).

$$L = K \lambda / \beta \cos \theta \quad (1)$$

where L is the crystallite size, λ is the X-ray wavelength in nanometer (nm), β is the peak width of the diffraction peak profile at half maximum height resulting from small crystallite size in radians and K is a constant related to crystallite shape, normally taken as 0.9.

More precisely, the full width at half height (FWHM) of the (110) characteristic diffraction plan was extracted to assess the crystallite size in the perovskite film and to compare between the different conditions (Table 1).

A lowest FWHM was obtained for the film using PEDOT: PSS as HTL layer, which suggests the presence of large crystals. In fact, a progressively low FWHM of XRD suggests that crystallite sizes have increased for the perovskite films coated on PEDOT: PSS from 23.88 nm to 26.40 nm, which confirms that the HTL layer can influence the nucleation and crystal growth processes of the perovskite film.

Table 1 The full width at half maximum (FWHM) of (110) diffraction peak extracted from the XRD patterns

Sample	FWHM($^\circ$)
PTAA/MAPbI _{3-x} Cl _x	0.336
PEDOT:PSS/MAPbI _{3-x} Cl _x	0.304

3.1.2 Scanning electron microscopy

The $\text{CH}_3\text{NH}_3\text{PbI}_{3-x}\text{Cl}_x$ perovskite films quality upon its growth on the two different HTL polymers (PEDOT:PSS and PTAA) is further examined by a scanning electron microscopy (SEM) measurement (Fig. 3). Furthermore, it has been shown that the efficiency of PSCs is directly correlates with the proper formation of the hybrid perovskite absorber layer.

Both samples shown a uniform and compact film with full surface coverage. On closer analysis of these two images, it is obviously clear that the PEDOT: PSS has considerably improved the nucleation and the growth of the perovskite film. The smoother perovskite layer deposited on the PEDOT: PSS has considerably larger grains with a sizes around 200 nm while that deposited on top of the PTAA has a grains sizes around 100 nm. The larger grain size is known to promote the electrical performance of the PSC device, by increasing the mobility of charge carriers and reducing the recombination pathways at the interfaces [34, 35].

Needle-like crystalline PbI_2 was observed at the grain boundaries for the perovskite film deposited on the PTAA, which is consistent with the increase of the PbI_2 peak intensity phase in the XRD pattern.

3.1.3 Optical properties

Since the nature of the HTL layer has strongly affect the crystallinity of the $\text{MAPbI}_{3-x}\text{Cl}_x$ perovskite film, we have after that examined the effect of the HTL layers on the optical properties of the perovskite film. First, we have studied the absorption of the $\text{MAPbI}_{3-x}\text{Cl}_x$ perovskite films deposited on each HTL layer. The UV–visible absorption spectra of the PTAA/MAPbI_{3-x}Cl_x and PEDOT: PSS/MAPbI_{3-x}Cl_x thin films are shown in Fig. 4a. It can be seen from the spectra that the perovskite thin films absorb a wide range of light from 400 to 800 nm. The two absorption spectra are similar, with a typical absorption at 740 nm [36] associated to the direct optical transition of the perovskite MAPbI_3 , a second transition around 490 nm associated to the direct optical transition of the lead-iodide octahedra PbI_6 [37]. It is evident that the strongest absorbance is obtained for the sample using the PEDOT: PSS as an HTL indicating the high quality of the perovskite layer which is in good agreement with the SEM measurements.

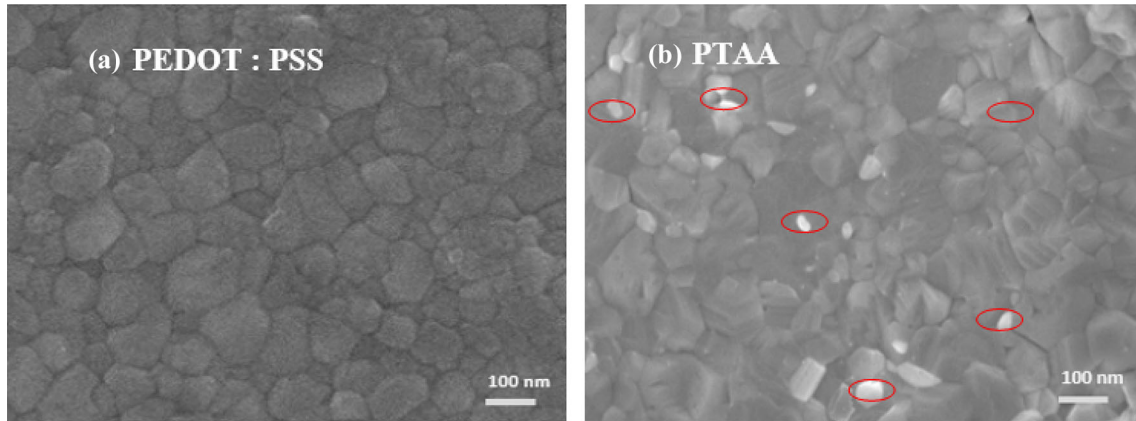


Fig. 3 SEM images of the MAPbI_{3-x}Cl_x perovskite structure grown on PEDOT: PSS **a** and PTAA **b** HTLs

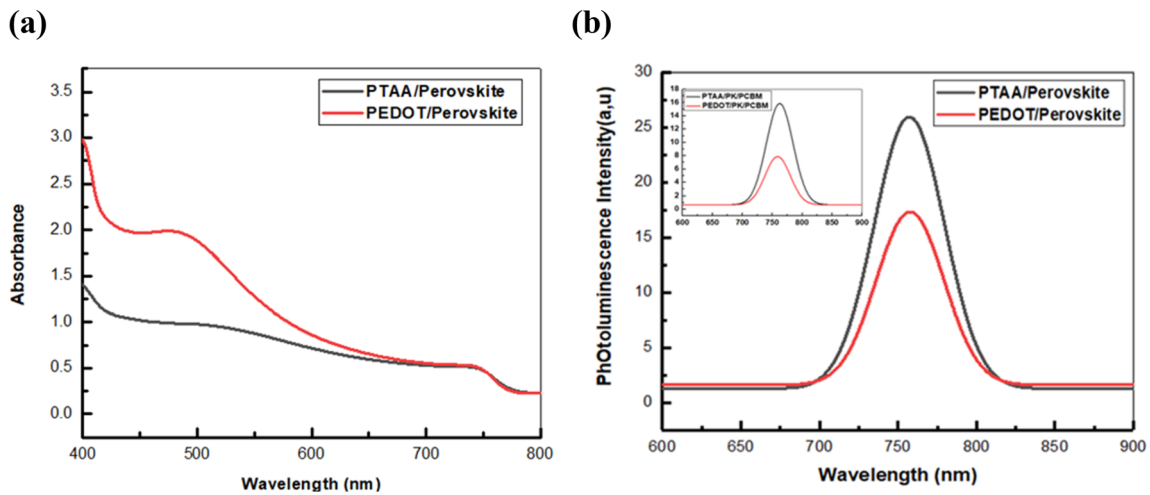


Fig. 4 **a** Absorbance spectra of MAPbI_{3-x}Cl_x films deposited on different HTL materials. **b** Photoluminescence spectra. The inset shows the PL spectra of perovskite films with a deposited PC₆₀BM layer

Furthermore, uniform perovskite film leads to greater absorption of sunlight which could affect the generation of the short circuit current and enhance the efficiency of the solar cells.

For further examination of the HTLs on the charge transfer and quench properties of the MAPbI_{3-x}Cl_x perovskite film, we have reported PL photoluminescence spectroscopy. Figure 4b shows the steady-state photoluminescence of the samples: Glass/ITO/PTAA/Perovskite and Glass/ITO/PEOT: PSS/Perovskite, under an excitation at 500 nm to predominantly excite the perovskite film. All the samples show a PL emission peaks centered in 760 nm which is due to the exciton emission. In addition, all the photoluminescence emission peaks show a slight shift towards the longest wavelength relative to the

absorptions peaks, which is known as the Stokes shift [38].

The steady-state PL spectrum of the film using the PEDOT: PSS showed slightly a decrease in the photoluminescence intensity than the sample based on PTAA which is proof of the low level of defects inside the perovskite layer and / or good quenching at the P-type layer interface [39, 40].

To better study the quenching efficiency the electron transport layer ETL (PC₆₀BM) was deposited on top the perovskite film. The quench properties was calculated using the following equation [41], While Where I₀ is the PL intensity before the deposit of the ETL layer and I is the PL intensity after the deposit of the ETL layer:

$$\eta = 1 - I/I_0$$

The values of these intensities are summarized in Table 1 in the support information. The excitons in the PTAA based film were 38% quenched, while 53% of the excitons were quenched in the film deposited on the PEDOT: PSS. This steady-state PL measurements indicate that the PEDOT: PSS had led to a more efficient PL quenching than the PTAA, implying that the holes separated from the photogenerated excitons within the perovskite layer are more efficiently extracted from perovskite to the PEDOT: PSS layer.

3.1.4 Photovoltaic performance

To further investigate the effect of the HTL layer on the performance of photovoltaic device, a series of perovskite solar cell with the configuration ITO/PEDOT: PSS/ MAPbI_{3-x}Cl_x/PC₆₀BM/BCP/Ag and ITO/PTAA/ MAPbI_{3-x}Cl_x/PC₆₀BM/BCP/Ag were elaborated, respectively. The photovoltaic parameters of the devices are summarized in Table 2, and the corresponding current density–voltage (J-V) curves scans of the champion devices are shown in Fig. 5.

A power conversion efficiency of 6.9% and 10.8% was achieved for the cells used the PTAA and PEDOT: PSS, respectively. The change in the HTL materials was found to have a significant impact on the device performance, especially in the FF and V_{OC} values. The devices with PEDOT layer exhibited a high FF of 57%, however for that based on the PTAA the FF was decreased to 46%. In order to understand the enhanced of the FF, the series resistance (R_S) and the shunt resistance (R_{Sh}) are also extracted for the two different holes materials. The R_S is originated from the materials used for fabrication of solar cells and the contact resistances, while the R_{Sh} is aroused from the leakage current of solar cells [42, 43]. For solar cells, it is of great importance to keep the R_S as small as possible since large R_S would lead to decreased J_{SC} and consequently low PCE. On the other hand, it is important to keep the R_{Sh} as large as possible since the small R_{Sh} would decrease the FF dramatically. The R_S estimated from the PSC with the PEDOT: PSS is around 3.6 Ω.cm², which is smaller than that from the PSC with the PTAA (4.9 Ω.cm²).

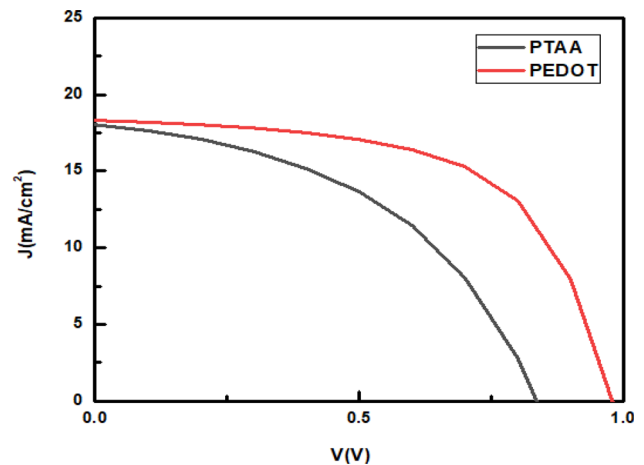


Fig. 5 J–V curves for the inverted PSCs having different HTLs

Further, the low PL obtained for such condition that indicate the good charge transfer from perovskite to HTL, could be linked to this lower series resistance.

In the other hand, the R_{Sh} is about 745 Ω.cm² for the PEDOT: PSS, which is larger than that of the PTAA (165 Ω.cm²). Thus, there is no wonder that the PEDOT: PSS possess suppressed leakage current, which consequently results in higher J_{SC} and FF.

Moreover, the high FF could be the consequence of the improvement of the crystallinity of the perovskite film, which is well confirmed by the XRD and SEM measurements. In fact, the large grain size estimated in the SEM image can reduce the grain boundaries and accordingly the recombination which increase the FF.

The enhancement of the V_{OC} could be attributed to the favorable energy level alignment between PEDOT: PSS and perovskite layer and to a reduced charge injection barrier at the PEDOT: PSS / Perovskite interface.

The study of the effect of the HTL material has shown that the PEDOT: PSS is much more adaptable as an HTL layer than the PTAA. We then became interested in studying the effect of the thermal annealing time of the PEDOT: PSS layer on the properties of our perovskite solar cells. A series of MAPbI_{3-x}Cl_x perovskites solar cells were elaborated

Table 2 Photovoltaic performance of the inverted PSCs

HTL material	V _{OC} (V)	J _{SC} (mA/cm ²)	FF (%)	PCE (%)	R _S (ohm.cm ²)	R _{Sh} (ohm.cm ²)
PTAA	0.829	18.0	46	6.9	4.95	165.63
PEDOT:PSS	0.931	19.7	57	10.8	3.88	530.21

with different annealing times of PEDOT: PSS at 180 °C for 15, 30 and 60 min.

3.2 Effect of PEDOT: PSS layer annealing time

3.2.1 Structural properties

In order to examine the effect of the annealing times of the PEDOT: PSS on the $\text{CH}_3\text{NH}_3\text{PbI}_{3-x}\text{Cl}_x$ films structure, XRD patterns are compared.

Figure 6a reveals the XRD diagrams of $\text{MAPbI}_{3-x}\text{Cl}_x$ deposited on top of ITO / PEDOT: PSS by one step spin coating and different annealing times of the PEDOT / PSS layer at 180 °C (15, 30 and 60 min). Diffraction peaks located at $2\theta = 17.5^\circ$ (110), 34.05° (220) and 37.53° (310) are obtained. Other low intensity peaks located at 15.4° and 30.7° corresponding to the PbI_2 phases were observed. All the samples are crystallized with the same tetragonal crystal structure. However, the diffraction intensities of the sample using the PEDOT: PSS annealing for 60 min was much higher than the other sample, which indicate that more MAPbI_3 perovskite phase has formed. In addition, this difference is the consequence of the change in the crystallization of the perovskite layer which was affected by annealing of the PEDOT: PSS layer.

In order to assess the crystallinity of the samples, the value of the FWHM for the main peak at 17.9° was extracted (Fig. 6b). A decrease in the values of FWHM is observed with the increase in the annealing time of the PEDOT: PSS layer from 0.590° to 0.307° .

As previously mentioned, the decrease in the value of FWHM is a sign of the increase in the crystal size perovskite film which was an increase from 16 to 30 nm.

3.2.2 Photoluminescence properties

An important conclusion about the recombination process of charge carriers can be extracted from a detailed photoluminescence (PL) analysis. Therefore Fig. 7 represents the steady-state photoluminescence (PL) Spectra of $\text{MAPbI}_{3-x}\text{Cl}_x$ perovskite film deposited on top of the PEDOT: PSS layer that was annealed at 180 °C for various times (15, 30 and 60 min), under an excitation wavelength of 500 nm.

By increasing the annealing time of the PEDOT: PSS layer, a blue shift of ~ 9 nm (from 760 to 751 nm) was observed. This behavior can be explained by the formation of unordered crystals. It has been previously reported that the PL emission shift was related with the crystallization of the perovskite material [16, 44, 45].

The PL intensity has been also affected by the variation of the PEDOT: PSS annealing time. In fact, the PL intensity of the perovskite elaborated on top of PEDOT: PS layer annealed for 60 min is observed to be stronger than the other samples. This behavior, confirming well suppressed of the non-radiative recombination which is associated with lower trap density and good crystallinity of the perovskite film [46].

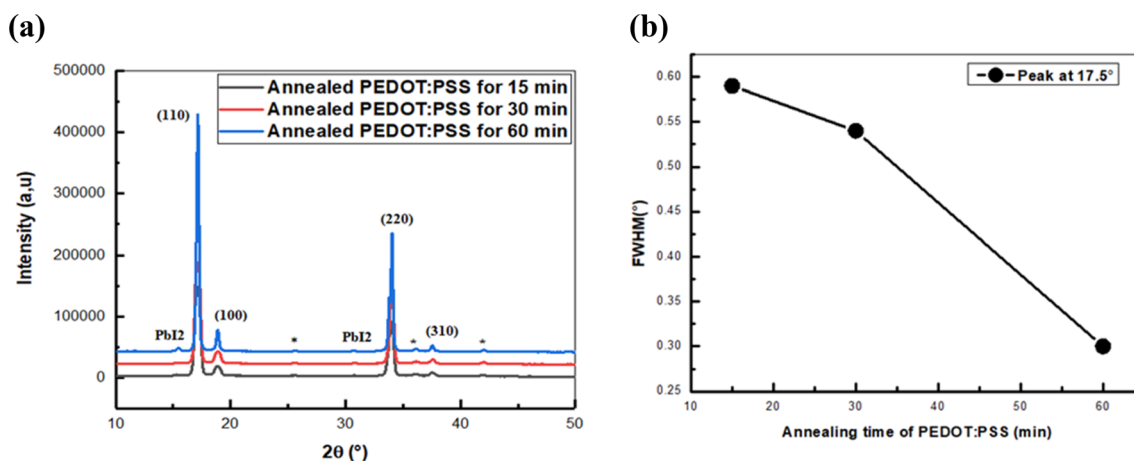


Fig. 6 **a** XRD patterns of perovskite films deposited on PEDOT: PSS annealed for different times, 15, 30 and 60 min. *peak attributed to ITO. **b** Variation of (110) peak Full Width at Half Maximum (FWHM) with the annealing times of PEDOT: PSS

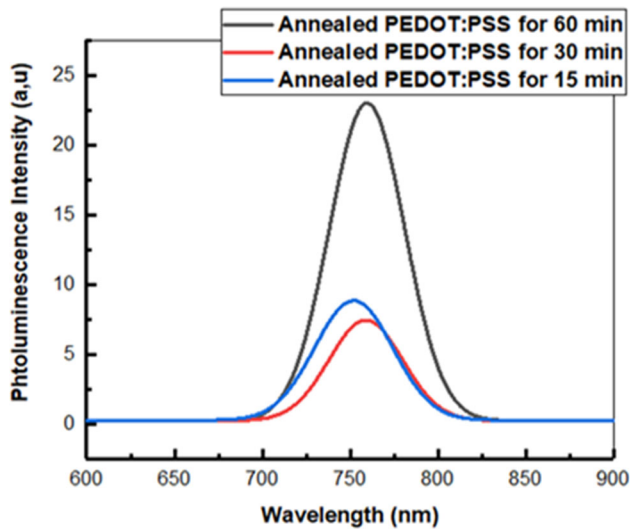


Fig. 7 Photoluminescence spectra of MAPbI_{3-x}Cl_x, deposited on the PEDOT: PSS thin film annealed for different times at 180 °C

3.2.3 Photovoltaic performance

The PEDOT: PSS layer was deposited as described in the experimental section and annealed at 180 °C for different annealing times followed by the subsequent deposition of the perovskite and the electron transport layer by one step spin coating. The current–voltage (*J*–*V*) characteristics measured under standard AM1.5G illumination (100 mW.cm⁻²) of these devices are presented in Fig. 8 and their corresponding photovoltaic parameters are summarized in Table 3. In order to study the annealing time effect

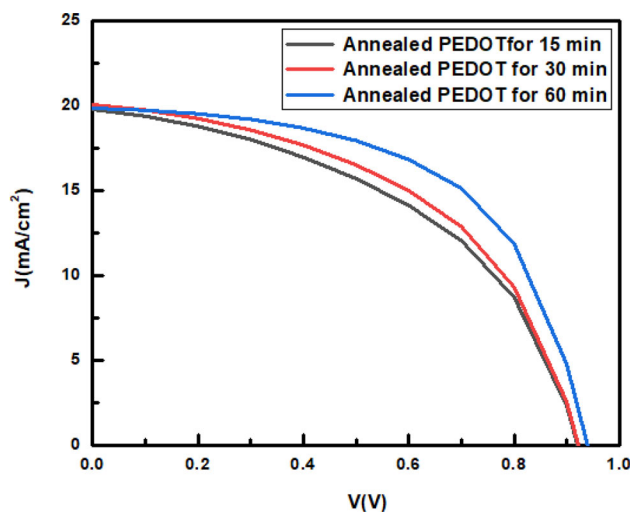


Fig. 8 *J*–*V* characteristics taken under standard AM1.5G illumination (100 mW.cm⁻²) for devices made using different annealing times of the PEDOT: PSS

of the PEDOT: PSS layer, all deposit parameters of the different layer are kept at the same. However, the annealing times of the PEDOT: PSS layer has varying from 15 min, 30 min to 60 min.

It is evident that the devices elaborated with a PEDOT: PSS layer annealed for a long time has the highest power conversion efficiency of 10.3% with *J*_{SC} of 19.7 mA/cm², *V*_{OC} of 0.931 V and FF of 57%. These improvements could be originated from lower recombination sites (due to a larger grain size) which is well confirmed by XRD and PL measurements. In contrast, the device fabricated with an HTL layer annealed at 180 °C for a short time has showed a low power conversion efficiency of 8.6% corresponding to a short circuit current density (*J*_{SC}) of 19.5 mA /cm², open circuit voltage (*V*_{OC}) of 0.907 V and fill factor (FF) of 48%. The main reason for this decrease in efficiency originates from the poor FF which is linked to poor shunt resistance and high series resistance.

It is evident that the devices elaborated with a PEDOT: PSS layer annealed for a long time has the highest power conversion efficiency of the order of 10.38% with *J*_{SC} of 19.75 mA /cm², a *V*_{OC} of 0.931 V and a FF of 57%. All these improvements be originated from the lower recombination sites (due to a larger grain size), which is well confirmed by the XRD and PL measurements. In contrast, the device fabricated with an HTL layer annealed at 180 °C for a short time has showed the lower power conversion efficiency of 8.6% corresponding to a short circuit current density (*J*_{SC}) of 19.5 mA / cm², an open circuit voltage (*V*_{OC}) of 0.907 V and a fill factor (FF) of 48%. The main reason for this decrease in efficiency originates from the poor FF which is linked to poor shunt resistance and high series resistance.

4 Conclusion

This research falls within the framework of the elaboration of inverted perovskite solar cells based on MAPbI_{3-x}Cl_x. The effects of the use of different HTL materials and different annealing time of the PEDOT: PSS layer on the perovskite films growth and devices efficiencies have been investigated in details. The results show that the properties, including absorption, photoluminescence, and crystallinity of perovskite films and device performance have been improved significantly by the use of the PEDOT: PSS as a HTL layer. Furthermore, a better charge transfer

Table 3 Photovoltaic performance parameters extracted from J–V measurements under standard AM1.5G illumination (100 mW.cm⁻²) of devices using different annealing times of PEDOT: PSS layer

Annealing time(min)	V _{OC} (V)	J _{SC} (mA/cm ²)	FF (%)	PCE (%)	RS (ohm.cm ²)	RSC (ohm.cm ²)
15	0.907	19.5	48	8.6	3.61	200.69
30	0.910	19.8	50	9.1	3.52	239.66
60	0.931	19.7	57	10.6	3.88	530.21

at the interface PEDOT: PSS/ MAPbI_{3-x}Cl_x has been obtained. We have also demonstrated that the performance of the device has been affected by the thermal annealing treatment of the PEDOT: PSS and that the best annealing time of the PEDOT: PSS at 180 °C is for 60 min resulting in good crystallinity of the perovskite film with less non-radiative recombination.

Funding

There is no funding to declare.

Data availability

All data generated or analyzed during this study are included in this published manuscript.

Declarations

Conflicts of interest There are no conflicts to declare.

Supplementary Information: The online version contains supplementary material available at <https://doi.org/10.1007/s10854-021-06666-z>.

References

- H. Tan et al., Efficient and stable solution-processed planar perovskite solar cells via contact passivation. *Science* **355**(6326), 722–726 (2017). <https://doi.org/10.1126/science.aai9081>
- L.V. Yinhu et al., Highly crystalline Nb-doped TiO₂ nanospindles as superior electron transporting materials for high-performance planar structured perovskite solar cells. *RSC advances* **8**(37), 20982–20989 (2018). <https://doi.org/10.1039/C8RA03559H>
- R. Lindblad et al., Electronic structure of CH₃NH₃PbX₃ perovskites: dependence on the halide moiety. *J. Phys. Chem. C* **119**(4), 1818–1825 (2015)
- A. Kojima et al., Organometal halide perovskites as visible-light sensitizers for photovoltaic cells. *J. Am. Chem. Soc.* **131**(17), 6050–6051 (2009)
- Green, Martin A., et al. 2020 “Solar cell efficiency tables (version 56).” *Progress in Photovoltaics: Research and Applications* 28.NREL/JA-5900–77544
- H. Zhou, Q. Chen, G. Li, S. Luo, T.B. Song, H.S. Duan, Z. Hong, J. You, Y. Liu, Y. Yang, *Science* **345**, 542–546 (2014)
- X. Zheng, B. Chen, J. Dai, Y. Fang, Y. Bai, Y. Lin, H. Wei, X.C. Zeng, J. Huang, *Nat. Energy* **2**, 17102 (2017)
- H. Mehdi, M. Matheron, A. Mhamdi, M. Manceau, C. Roux, S. Berson, A. Bouazizi, *J. Mater. Sci.: Mater Electron* (2020). <https://doi.org/10.1007/s10854-020-03571-9>
- J. You, L. Meng, T. Song, T. Guo, Y.M. Yang, W. Chang, Z. Hong, H. Chen, H. Zhou, Q. Chen, Y. Liu, N. DeMarco, Y. Yang, *Nat. Nanotechnol.* **11**, 75–81 (2015)
- M. Saliba, T. Matsui, J.Y. Seo, K. Domanski, J.P. Correa-Baena, M.K. Nazeeruddin, S.M. Zakeeruddin, W. Tress, A. Abate, A. Hagfeldt, M. Grätzel, *Energy Environ. Sci.* **9**, 1989–1997 (2016)
- H. Mehdi, A. Mhamdi, A. Bouazizi, Effect of perovskite precursor ratios and solvents volume on the efficiency of MAPbI_{3-x}Cl_x mixed halide perovskite solar cells. *Mater. Sci. Semicond. Process.* **109**, e104915 (2020)
- N.J. Jeon, H. Na, E.H. Jung, T.-Y. Yang, Y.G. Lee, G. Kim, H.-W. Shin, S. Seok, J. Lee, J. Seo, *Nat. Energy* **3**, 682 (2018)
- L. Meng, J. You, T.-F. Guo, Y. Yang, *Acc. Chem. Res.* **49**, 155 (2016)
- Y. Zhang et al., Charge selective contacts, mobile ions and anomalous hysteresis in organic–inorganic perovskite solar cells. *Mater. Horizons* **2**(3), 315–322 (2015)
- A.H. Ghahremani, B. Martin, A. Gupta, J. Bahadur, K. Ankireddy, T. Druffel, Rapid fabrication of perovskite solar cells through intense pulse light annealing of SnO₂ and triple cation perovskite thin films. *Mater. Des.* **185**, e108237 (2020)
- A. Khorasani, M. Marandi, N. Taghavinia, Application of combinative TiO₂nanorods and nanoparticles layer as the

- electron transport film in highly efficient mixed halides perovskite solar cells. *Electrochim. Acta* **297**, 1071–1078 (2019)
17. H. Mehdi, A. Mhamdi, R. Hannachi, A. Bouazizi, MAPbBr₃ perovskite solar cells via a two-step deposition process. *RSC Adv.* **9**(23), 12906–12912 (2019)
 18. W. Kim, J. Park, H. Kim, Y. Pak, H. Lee, G.Y. Jung, Sequential dip-spin coating method: fully infiltration of MAPbI₃-xCl_x into mesoporous TiO₂ for stable hybrid perovskite solar cells. *Electrochim. Acta* **245**, 734–741 (2017)
 19. H. Mehdi, A. Mhamdi, A. Bouazizi, Effect of annealing treatment on the properties of inverted solar cells based on mixed halide perovskite. *Phys. E: Low-dimens. Syst. Nanostructures* **119**, e114000 (2020)
 20. L.C. Chen, C.C. Chen, J.C. Chen, C.G. Wu, Annealing effects on high-performance CH₃NH₃PbI₃ perovskite solar cells prepared by solution-process. *Sol. Energy* **122**, 1047–1051 (2015)
 21. A. Mathur, A. Li, V. Maheshwari, Nanoscale architecture of polymer-organolead halide perovskite films and the effect of polymer chain mobility on device performance. *J. Phys. Chem. Lett.* **12**(5), 1481–1489 (2021)
 22. R. Saraf, A. Mathur, V. Maheshwari, Polymer-controlled growth and wrapping of perovskite single crystals leading to better device stability and performance. *ACS Appl. Mater. Interfaces.* **12**(22), 25011–25019 (2020)
 23. A. Abrusci, S.D. Stranks, P. Docampo, H.-L. Yip, A.K.-Y. Jen, H.J. Snaith, *Nano Lett.* **13**, 3124 (2013)
 24. D.Y. Lee, S.I. Na, S.S. Kim, Graphene oxide/PEDOT: PSS composite hole transport layer for efficient and stable planar heterojunction perovskite solar cells. *Nanoscale* **8**(3), 1513–1522 (2016)
 25. W. Yan, S. Ye, Y. Li, W. Sun, H. Rao, Z. Liu, Z. Bian, C. Huang, *Adv. Energy Mater.* **6**, 1600474 (2016)
 26. A. Fakhruddin, L. Schmidt-Mende, G. Garcia-Belmonte, R. Jose, I. Mora-Sero, *Adv. Energy Mater.* **7**, 1700623 (2017)
 27. N.J. Jeon, H. Na, E.H. Jung, T.Y. Yang, Y.G. Lee, G. Kim, J. Seo, A fluorene-terminated hole-transporting material for highly efficient and stable perovskite solar cells. *Nat. Energy* **3**(8), 682–689 (2018)
 28. Z.L. Tseng, L.C. Chen, C.H. Chiang, S.H. Chang, C.C. Chen, C.G. Wu, Efficient inverted-type perovskite solar cells using UV-ozone treated MoO_x and WO_x as hole transporting layers. *Sol. Energy* **139**, 484–488 (2016)
 29. Y. Guo, X. Yin, J. Liu, W. Chen, S. Wen, M. Que, W. Que, Effect of the post-annealing temperature on the thermal-decomposed NiO_x hole contact layer for perovskite solar cells. *J. Adv. Dielectr.* **8**(01), 1850006 (2018)
 30. K. Weijun et al., Dopant-free tetrakis-triphenylamine hole transporting material for efficient tin-based perovskite solar cells. *J. Am. Chem. Soc.* **140**(1), 388–393 (2018)
 31. H. Chen, W. Fu, C. Huang, Z. Zhang, S. Li, F. Ding, H. Chen, Molecular engineered hole-extraction materials to enable dopant-free, efficient p-i-n perovskite solar cells. *Adv. Energy Mater.* **7**(18), 1700012 (2017)
 32. M.S. Al-Buriahi, C. Sriwunkum, H. Arslan, B.T. Tonguc, M.A. Bourham, Investigation of barium borate glasses for radiation shielding applications. *Appl. Phys. A* **126**(1), 1–9 (2020)
 33. M. Ahmed et al., The main role of thermal annealing in controlling the structural and optical properties of ITO thin film layer. *Opt. Mater.* **113**, e110866 (2021)
 34. C. Wang et al., "Air-induced high-quality CH₃NH₃PbI₃ thin film for efficient planar heterojunction perovskite solar cells. *J. Phys. Chem. C* **121**(12), 6575–6580 (2017)
 35. N. Zhou et al., CsI pre-intercalation in the inorganic framework for efficient and stable FA_{1-x}Cs_xPbI₃ (Cl) perovskite solar cells. *Small* **13**(23), 1700484 (2017)
 36. T.J. Jacobsson, J.P. Correa-Baena, E. HalvaniAnaraki, B. Philippe, S.D. Stranks, M.E. Bouduban, H. Rensmo, Unreacted PbI₂ as a double-edged sword for enhancing the performance of perovskite solar cells. *J. Am. Chem. Soc.* **138**(32), 10331–10343 (2016)
 37. A. Khorasani, M. Maziar, N. Taghavinia, Application of combinative TiO₂nanorods and nanoparticles layer as the electron transport film in highly efficient mixed halides perovskite solar cells. *Electrochimica Acta* **297**, 1071–1078 (2019)
 38. X. Song, W. Wang, P. Sun, W. Ma, Z.K. Chen, Additive to regulate the perovskite crystal film growth in planar heterojunction solar cells. *Appl. Phys. Lett.* **106**(3), e033901 (2015)
 39. P.W. Liang, C.C. Chueh, X.K. Xin, F. Zuo, S.T. Williams, C.Y. Liao, A.K.Y. Jen, High-performance planar-heterojunction solar cells based on ternary halide large-band-gap perovskites. *Adv. Energy Mater.* **5**(1), 1400960 (2015)
 40. S. Sanchez, N. Christoph, B. Grobety, N. Phung, U. Steiner, M. Saliba, A. Abate, Efficient and stable inorganic perovskite solar cells manufactured by pulsed flash infrared annealing. *Adv. Energy Mater.* **8**(30), 1802060 (2018)
 41. J.R. Albani, *Principles and Applications of Fluorescence Spectroscopy* (John Wiley & Sons, 2008)
 42. Z. Zhu, Y. Bai, T. Zhang, Z. Liu, X. Long, Z. Wei, S. Yang, High-performance hole-extraction layer of sol-gel-processed NiO nanocrystals for inverted planar perovskite solar cells. *Angewandte Chemie* **126**(46), 12779–12783 (2014)
 43. X. Huang, K. Wang, C. Yi, T. Meng, X. Gong, Efficient perovskite hybrid solar cells by highly electrical conductive PEDOT: PSS hole transport layer. *Adv. Energy Mater.* **6**(3), 1501773 (2016)
 44. V. D'Innocenzo, A.R.S. Kandada, M. De Bastiani, M. Gandini, A. Petrozza, Tuning the light emission properties by band

- gap engineering in hybrid lead halideperovskite. *J. Am. Chem. Soc.* **51**, 17730–17733 (2014)
45. K. Wu, A. Bera, C. Ma, Y. Du, Y. Yang, L. Li, T. Wu, Temperature-dependent excitonic photoluminescence of hybrid organometal halide perovskite films. *Phys. Chem. Chem. Phys.* **16**(41), 22476–22481 (2014)
46. A. Mhamdi, H. Mehdi, A. Bouazizi, G. Garcia-Belmonte, One-step methylammonium lead bromide films: Effect of annealing treatment. *J. Mol. Struct.* **1192**, 1–6 (2019)

Publisher's Note Springer Nature remains neutral with regard to jurisdictional claims in published maps and institutional affiliations.